Heat dissipation at a graphene–substrate interface

2012 J. Phys.: Condens. Matter 24 475305

(http://iopscience.iop.org/0953-8984/24/47/475305)

IOP PUBLISHING JOURNAL OF PHYSICS: CONDENSED MATTER
J. Phys.: Condens. Matter **24** (2012) 475305 (7pp) doi:10.1088/0953-8984/24/47/475305

Heat dissipation at a graphene–substrate interface

Zhiping Xu[1,2] **and Markus J Buehler**[2]

[1] Department of Engineering Mechanics and Center for Nano- and Micro-Mechanics, Tsinghua University, Beijing 100084, People's Republic of China
[2] Laboratory for Atomic and Molecular Mechanics, Department of Civil and Environmental Engineering, Massachusetts Institute of Technology, Cambridge, MA 02139, USA

E-mail: xuzp@tsinghua.edu.cn and mbuehler@MIT.EDU

Received 28 July 2012, in final form 17 September 2012
Published 2 November 2012
Online at stacks.iop.org/JPhysCM/24/475305

Abstract
The development of nanoelectronics faces severe challenges from Joule heating, leading to high power density and spatial localization of heat, which nucleates thermal hot spots, limits the maximum current density and potentially causes catastrophic materials failure. Weak interfacial coupling with the substrate is a major route for effective heat mitigation in low-dimensional materials such as graphene and carbon nanotubes. Here we investigate the molecular-scale physics of this process by performing molecular dynamics simulations, and find that significant heating in graphene supported by a silicon carbide substrate cannot be avoided when the areal power density exceeds $P_G = 0.5$ GW m^{-2}. A steady state will be established within 200 ps with a significant temperature difference built up across the interface, and the interfacial thermal conductivity κ_c increases at higher power densities from 10 to 50 MW m^{-2} K^{-1}. These observations are explained by a two-resistor model, where strong phonon scattering at the interface may perturb the ballistic heat transport and lead to a diffusive mechanism. Nanoengineering the interfacial thermal coupling by intercalating guest atoms shows potential for designing thermally transparent but electronically insulating interfaces, which paves the way for simultaneously optimizing thermal management and charge carrier mobility in nanoelectronics.

(Some figures may appear in colour only in the online journal)

1. Introduction

Nanoelectronics, built with nanoscale low-dimensional materials such as graphene and carbon nanotubes, holds great promises for the next-generation of nanoelectromechanical systems (NEMS) and information technology, contributing towards continuing the miniaturization of devices and for maintaining Moore's law. Numerous results reported in recent years indicate promising features including ultrahigh charge mobility (>10 000 cm^2 V^{-1} s^{-1} at room temperature) [1], strong suppression of weak localization [2], sensibility to environmental cues [3], outstanding thermal and mechanical stabilities [4], and many others. While carbon nanostructures such as graphene and carbon nanotubes begin to play important roles, their performance is limited by a number of energetic issues during operation. At high current, the electron flow will induce significant overpopulation of phonons, impeding transport and enhancing scattering with electrons as a result of strong electron–phonon interactions. Moreover, a local temperature increase resulting from Joule heating creates local hot spots confined to nanoscale dimensions, especially at defective sites. According to recent reports, the power density in these nanoelectronic transistors and circuits could approach very high values beyond 1 GW m^{-3} [5, 6]. This excess amount of thermal energy, if not dissipated efficiently, could result in breakdown in performance, nucleation of defects, reconstruction of surfaces and interfaces, and even materials failure [7, 8]. Moreover, in many other applications including nanoelectromechanical devices and photovoltaic cells, localized heat accumulation also plays a critical role and effective thermal management, especially between nanostructures and their environments (substrates, electrodes, air, etc), is critical [9].

Graphene, a monatomic layer material, is routinely supported by an insulating substrate and in close contact with metallic electrodes for electronic device applications. The substrate, in addition to free surfaces and electrodes, becomes a major path to dissipate heat generated in a device. The thermal radiation into open space is calculated to be negligible, and the substrate underneath the graphene sheet is reported to be responsible for 77% of the total heat dissipation to substantially reducing the operating temperature [5]. Raman scattering microscopy [5, 10] and ultrafast optical pump–probe spectroscopy techniques [11] were used to track the energetic map at the interface between graphene and silicon dioxide. The interfacial resistances were measured to vary within the bounds for metal–semiconductor interface, i.e. between 20 and 110 MW m^{-2} K^{-1} [11]. Electron–phonon coupling and its impact on the device performance were also discussed. However, the atomistic mechanism for the thermal energy transfer at this interface, especially its dependence on the interfacial structure has not been clarified. It can be clearly seen from figure 1(a) that although the bulk thermal conductivities of silicon carbide, silica and graphite differ by 3–4 orders of magnitude, their interfacial thermal conductivity as measured show much less contrast. This suggests that the atomic structure and interaction control interfacial thermal transfer, in addition the bulk properties of materials further away from the interface as described in conventional models such as acoustic the mismatch model (AMM) and the diffusive mismatch model (DMM) [12]. Moreover, the interfacial chemistry is also of extreme importance for the behavior of nanoelectronical systems. An electrically insulating but thermally transparent interface is the key for high-performance electronic devices, as a strongly coupling between nanostructures and the substrate enhance the heat dissipation, but also induces a drag on charge carriers, reduces their mobility and results in a trade-off between thermal management and mobility. Recently, various approaches were reported to modify the interface between graphene and the substrate by intercalating metal atoms [13], gases (e.g. O_2) [14], or hydrogen termination [15]. These techniques propose a new dimension for interfacial engineering, in addition to selecting substrate materials. It is thus interesting to explore their potential in thermal management.

In this work, the thermal dissipation through a graphene–substrate interface in nanoelectronics is explored by performing empirical molecular dynamics (MD) simulations. The interfacial thermal resistance between graphene and the substrate is characterized, and the temperature evolution in transient simulations are tracked and discussed. For a graphene sheet on the $(000\bar{1})$ surface of 6H-SiC (figure 1(b)), a heat power with areal density P is generated within the supported graphene sheet to model a delocalized Joule heating source. In the steady state, a heat flux $J = P$ is transferred through its interface to the substrate. We explore the heat dissipation process with P in a typical range of nanoelectronics applications from 0.1 to 100 GW m^{-2}. Within this range, the graphene structures in our simulations are observed to be preserved under heating. In recent work we investigated the interfacial electronic and phononic coupling

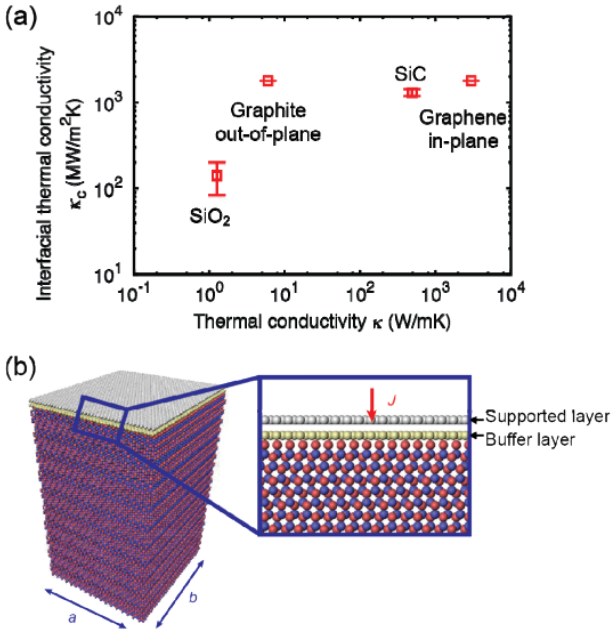

Figure 1. Thermal transport across interfaces with graphitic structures. (a) Thermal conductivity κ and interfacial thermal conductivity κ_c of several representative materials and their interfaces with graphene or carbon nanotubes [33–36]. (b) A schematic illustration and the atomic structure of graphene–6H-SiC interface.

at various graphene–substrate systems [16, 17]. For the sake of a complete picture in understanding the underlying energetic processes in nanoelectronics, here we focus on the mechanisms of phononic coupling and heat transfer between the graphene sheet and a 6H-SiC substrate. Silicon carbide is chosen here not only because of it is common used in graphene-based electronics, but also due to the fact that high-quality SiC–epitaxial graphene is able to be fabricated on the wafer scale routinely [18, 19]. Although there is additional energy flow from the graphene sheet into the substrate through surface phonon scattering in the hot electron regime, our approach leads to fundamental insights into phonon-based interfacial energy transfer during device operation.

2. Materials and methods

The interface between graphene and 6H-SiC is constructed at a C-terminated $(000\bar{1})$ SiC surface, which reconstructs as $(3\sqrt{3} \times 3\sqrt{3})R30°$ and coincides with a 13 × 13 graphene supercell (figure 1(b)). The graphene sheet is deposited, through van der Waals interactions, on the reconstructed graphene buffer layer, which is covalently bonded with silicon atoms downwards. The height of the 6H-SiC substrate is 15.1 nm, which is tested to be large enough in tracking the thermal runaway. A supercell of $a = 3.2$ nm $b = 5.5$ nm is used in the lateral direction. Open boundary conditions are used in the directions normal to the interface. In our supercell approach, phonon modes with longer in-plane wavelengths are ignored. However, as the focus is placed on the heat transfer across the interface, the lateral spatial confinement is not expected to play an important role. This is verified by

performing MD simulations with a 2×2 supercell, where the results do not show significant difference between these two systems.

The interatomic interactions in 6H-SiC and supported graphene are described using Tersoff and adaptive intermolecular reactive empirical bond order (AIREBO) potential functions, respectively [20]. The non-covalent van der Waals interactions between the graphene sheet and the 6H-SiC substrate (including the buffer layer) are expressed in a Lennard-Jones type function with parameters $\sigma_{C-C} = 3.234$ nm, and $\varepsilon_{C-C} = 0.003\,13$ eV [21]. The Tersoff and AIREBO potential functions and parameters are known to give reasonable predictions for structural, mechanical and thermal properties of both graphene and 6H-SiC [22, 23], although it should be kept in mind that these bond order potential functions were reported to underestimate the dispersion of ZA phonons in graphene and thus could affect the predictions of interfacial thermal conductivities [24–26]. All MD simulations are performed using the large-scale atomic/molecular massively parallel simulator (LAMMPS) package [27]. The step for time integration is 0.5 fs. When argon atoms are intercalated between the supported and buffer layers in the simulations, a Lennard-Jones potential function with parameters $\varepsilon_{Ar-Ar} = 3.405$ nm and $\sigma_{Ar-Ar} = 0.010\,3235$ eV is used, and a mixing rule is used to model the interactions between argon and carbon atoms, i.e. $\varepsilon_{C-Ar} = (\varepsilon_{C-C}\varepsilon_{Ar-Ar})^{1/2}$ and $\sigma_{Ar-Ar} = (\sigma_{C-C} + \sigma_{Ar-Ar})/2$.

The hybrid graphene–6H–SiC system is first equilibrated by coupling to a Berendsen thermostat at 300 K. To simulate Joule heating, non-translational kinetic energy is added to carbon atoms in the graphene sheet by scaling the velocities of atoms, equally in the x, y and z directions. This treatment does not consider the phonon spectrum of energy loss by electrons, which is known to occur mainly through LA phonons, followed by TA phonons. To investigate this artificial effect, similar simulations are also performed by scaling only in-plane kinetic energy of atoms in the x and y directions. The results do not show a quantitative difference in both the temperature evolution and interfacial thermal conductivity, thus our following discussion will be based on the former approach. The temperature in the supported graphene sheet, the buffer layer and the temperature field $T(x)$ of the whole system is tracked by averaging both temporally (every 100 ps) and spatially in 0.1 nm thick slabs along the coordinate x, in the depth direction. The temperature of a 2 nm thick slab in the bottom of 6H-SiC substrate is coupled to a Berendsen thermostat at 300 K during the simulations as a heat sink.

3. Results and discussion

3.1. Transient heat dissipation process

As heat dissipation through radiation or air-cooling is neglected, thermal transfer across the interfaces with the substrate and electrodes are the only routes. We focus on the first one here by exploring the interface with silicon carbide as it usually has a much larger contact area than the electrodes. The time evolution of local temperature in both the supported graphene sheet (T_G) and the buffer graphene layer (T_B) in 6H-SiC substrate, between which there is an interface interacted through van der Waals interactions, is plotted in figure 2. After heat is continuously generated in the supported graphene sheet, T_G first rises up rather rapidly (within hundreds of picoseconds), when the rate of heating or areal power density is higher than a critical value $P_G = 0.5$ GW m^{-2}. For $P < P_G$, T_G cannot be distinguished from T_B and both fluctuate with an amplitude of tens of Kelvin around the environmental temperature $T = 300$ K. These results suggest that the generated thermal flux is heavily localized in the graphene sheet and thermal dissipation through the interface is not activated for P exceeding P_G.

The results depicted in figure 2 also reveal a characteristic time scale τ for the supported graphene sheet that is heated up. Below $P = 10$ GW m^{-2}, T_G rises within $\tau = 250$ ps before reaching the steady state. While for $P > 10$ GW m^{-2}, τ decreases gradually from 200 to 100 ps. This time scale defines the maximum duration a high-power heat pulse could last without inducing damage to the device. Moreover, when P is less than $P_B = 5$ GW m^{-2}, the materials in buffer layer and substrate are not significantly heated and T_B stays well below 310 K. In contrast, when P exceeds this critical value P_B, T_B increases slightly and approaches 604 K for $P = 100$ GW m^{-2}. When $t > \tau$, a steady state of the device is established, and there is eventually a temperature difference and gradient built up across the interface and in the substrate respectively. This interface-limited regime of heat dissipation highlights the key importance of interfaces between nanostructures and the environment in improving thermal management of powered graphene-based electronic devices.

When exposed to ambient air, electrical breakdown will occur by oxidation at 600 °C. While operating in the vacuum the breakdown temperature of graphene increases to 3600 °C, the structural and thermal stability of suspended graphene will be lost [4, 28]. Defects and open edges in graphene nanostructures as implemented in electronics and electromechanical devices will further lower this critical temperature, and structural failure will occur and leads to unrecoverable catastrophic damage. For example, desorption of carbon dimers from graphene nanoribbons is expected to occur at 2500 K [29]. The values of T_G and T_B in the steady states are summarized in figure 3(a), which shows a gradually increasing trend, and T_G will exceed 900 K at $P > 10$ GW m^{-2} and 2000 K at $P > 50$ GW m^{-2}. Based on these results the temperature window for stable operation of graphene-based electronic devices can be predicted. Moreover, after the steady state is reached, the interfacial thermal conductivity κ_c or Kapitza conductivity between the supported graphene sheet and 6H-SiC substrate can be calculated from its definition $\kappa_c = J/A\Delta T$, where J is the heat flux across interface that equals to the areal power density P here in the steady state, A is the contact area, and $\Delta T = T_G - T_B$ is the temperature difference across the interface. The results shown in figure 3(b) shows that κ_c has a value on the order of 10 MW m^{-2} K^{-1}. A distinct dependence of κ_c on the power density or temperature difference across the interface

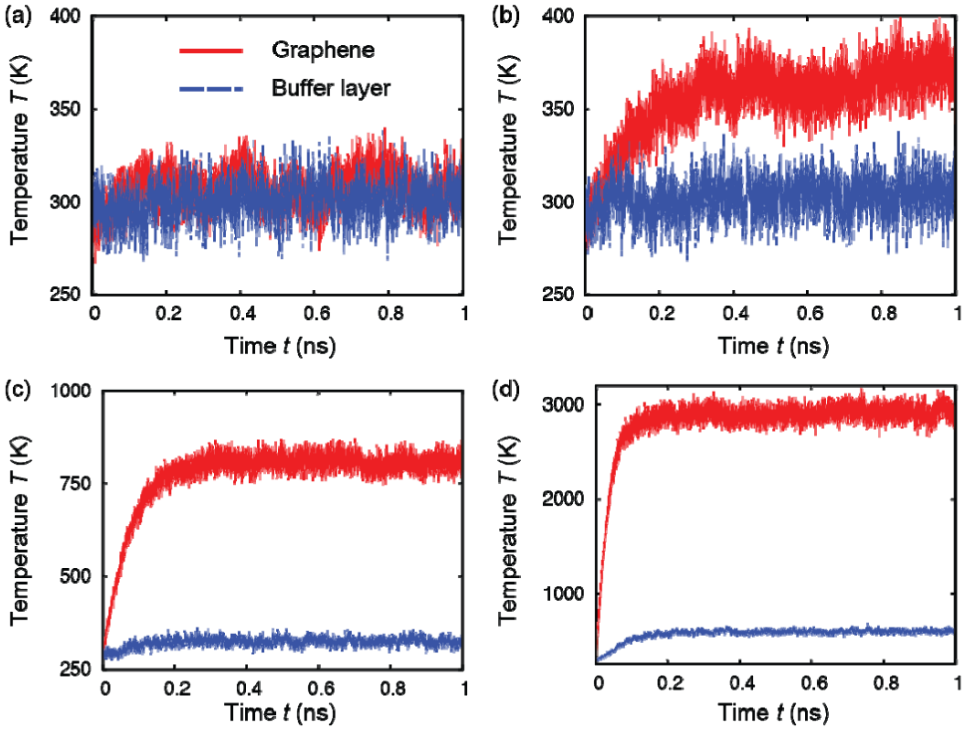

Figure 2. Profiles of temperature evolution in the graphene sheet T_G (red) and buffer layer T_B (blue) in the 6H-SiC substrates. The heat flux generated in the supported graphene sheet P is (a) 0.1, (b) 1.0, (c) 10.0 and (d) 100.0 GW m^{-2}, respectively. The results show that after a heating duration of about 200 ps, a steady state is then reached with a temperature difference established between T_G and T_B created for P exceeds $P_G = 0.5$ GW m^{-2}.

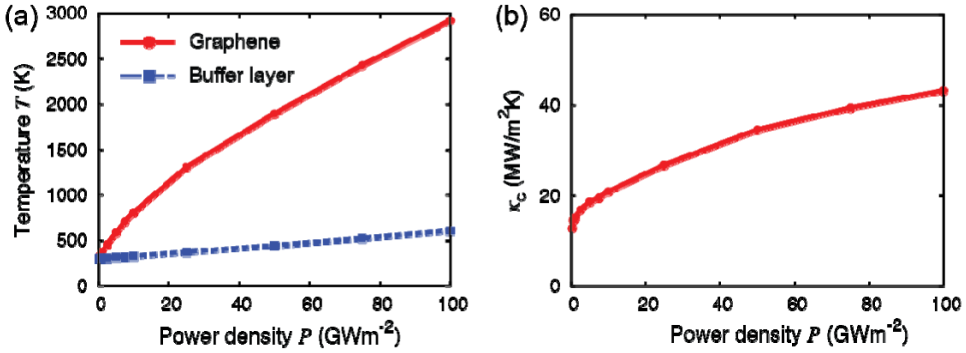

Figure 3. Power density dependent interfacial thermal conductivity. (a) The temperature evolution in the graphene sheets at various power density P from 0.1 to 100 GW m^{-2}. (b) Interfacial thermal conductivity between graphene and 6H-SiC substrate as calculated from $\kappa_c = J/(\Delta TA)$, where ΔT is the temperature difference across the interface with area A.

is observed. As P increases from 0.1 to 100 GW m^{-2}, κ_c increases quickly first and then more gradually from 12.81 to 43.23 MW m^{-2} K^{-1}. This can be explained as more phonon modes are occupied, and phononic coupling between the graphene sheet and substrate are enhanced at an elevated temperature to advance heat transfer across the interface.

For comparison, the interfacial thermal conductivity between graphene and the 6H-SiC substrate is also investigated here through steady-state non-equilibrium MD simulations (NEMD) following the Müller-Plathe approach [30]. A graphene sheet sandwiched between two 6H-SiC materials is constructed as the model with lateral dimensions of 3.2 × 5.54 nm^2 and a total length of 25 nm, i.e. one interface is formed that includes two contacts between graphene and buffer layers in silicon carbide are created. The momentum exchanges take place in two slabs of silicon carbide with thickness of 1 nm. The frequency is controlled to maintain a temperature difference between the heat source and sink below 100 K. The contact resistance at this interface is calculated to be $\kappa_c = 82$ MW m^{-2} K at 300 K, which is consistent to what we obtained from the transient simulations reported earlier (figure 3(b)), and simulation results for other van der Waals interfaces discussed in earlier works [12, 31]. The difference in numbers identified here could be due to the treatment of heating in transient simulations by scaling velocities of atoms directly, rather than modeling them as infrequent elastic collisions in NEMD simulations. Also the different setups in the transient simulations with one-side

contact and NEMD simulations with a 'sandwich structure' could affect the prediction of κ_c. This value of contact resistance indicates a Kapitza length $l_c = \kappa_{SiC}/\kappa_c$ on the order of ten micrometers if the thermal conductivity of silicon carbide $\kappa_{SiC} = 330.27$ W m^{-1} K is used [32].

3.2. Graphene-based electronic devices

A summary of thermal conductivities κ in bulk materials and interfacial thermal conductivity κ_c is presented in figure 1(a). Interestingly, it can be seen that although κ in several solids listed could differ by several orders of magnitude, the values of κ_c at their interfaces with graphene or carbon nanotubes do not have the same amplitude of discrepancy and are narrowly distributed in an interval around 100–1000 MW m^{-2} K^{-1}. For example, the experimental measured thermal conductivity of 6H-SiC is $\kappa_{SiC} = 330.27$ W m^{-1} K^{-1}, while for quartz and fused silica, $\kappa_{SiO_2} = 1.3$ and 1.4 W m^{-1} K^{-1}, respectively [32]. However, their interfacial thermal conductivity with graphene is measured experimentally to be 1303.55 and 141.7 MW m^{-2} K^{-1}, respectively [11, 33–35]. This comparison indicates that interfacial scattering of heat carriers plays a dominating role in determining the interfacial thermal conductivity. Additionally, we compare these κ_c values with the one for the interface in graphite, which is 1800 W m^{-2} K^{-1}. This suggests that although they feature the same van der Waals based interactions, heat transfer between the same material (here, graphene), has a higher interfacial thermal conductivity [12, 36].

Hot spots in graphene-based nanoelectronics can also be avoided by limiting the duration of heating (e.g. electronic, laser, etc), according to the temperature profile plotted in figure 2. When a short heat pulse with areal power density $P = 1$ GW m^{-2} is generated in the graphene sheet, e.g. for 50 and 100 ps, we find that the highest temperature that can be reached is well below 550 and 700 K, respectively (figure 4). After the heat pulse source is released, temperature in graphene sheet decays exponentially within 500 ps. The decaying profiles are also used to calculate the interfacial thermal conductivity [31], which gives $\kappa_c = 8.29$ and 9.35 MW m^{-2} K^{-1}, respectively, which agree with aforementioned results using other methods.

We also investigate heat dissipation at the interfaces between graphene and electrodes such as copper contacts, which shows similar trends that the temperature increase in the supported graphene layer is manifested in hundreds of picosecond. However, electronic coupling at the interface could help to elevate heat dissipation efficiency. In empirical MD simulations, electrons as carriers of heat are not considered. Although previous experiments suggest that phononic contribution dominates at interfaces between carbon nanostructures and metal contacts, further exploration should be carried out to address heat transfer at graphene–metal contacts, possibly based on a interfacial version of the Wiedemann–Franz law, which was recently proposed and validated [37, 38].

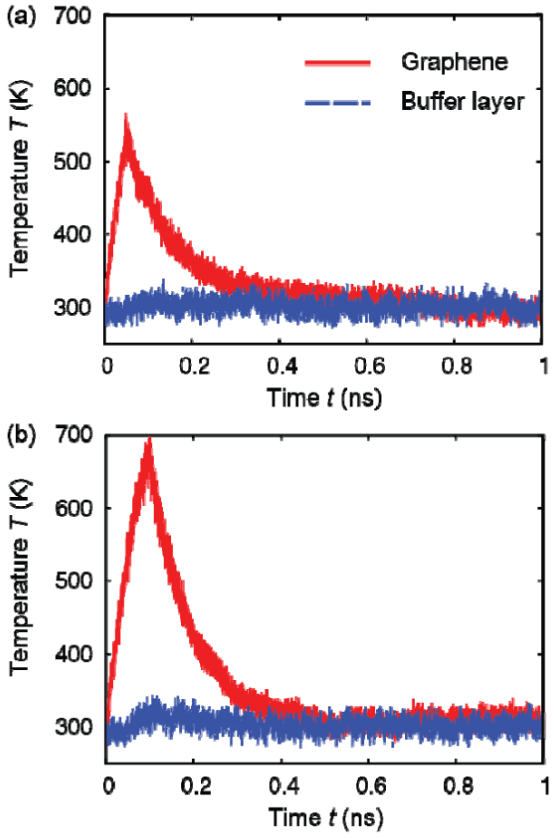

Figure 4. Temperature evolution profiles in the graphene sheet and buffer layer after short heat pulses $P = 10$ GW m^{-2} are generated for (a) 50 ps and (b) 100 ps. The exponential decay of temperature in the graphene sheet is fitted to calculate the interfacial thermal conductivity.

3.3. A two-resistor model

To obtain more insights from the simulation results, we develop a two-resistor model where the interface and 6H-SiC substrate are represented as two serially connected resistors, as illustrated in figure 5(a). Joule heating and thermostating at the bottom substrate layer are considered here as heat sources and sink through introducing appropriate boundary conditions. The result shows $\Delta T = (dT/dx)\kappa_{SiC}/\kappa_c$, where dT/dx is the temperature gradient in the substrate, and the temperature where heat flux is generated increases first and then reaches a steady state. Results from this simple model are based on the assumption of Fourier's diffusive heat transfer regime, where resistors are additive. We note that the results shown in figures 5(b) and (c) are qualitatively consistent with our MD simulation results (figure 5(d)), which suggest diffusive heat dissipation in the substrate. According to recent progress in nanoscale heat conduction, non-Fourier models that include the ballistic, or wave-like, nature of heat, such as the Cattaneo two-temperature model, have been suggested to provide better predictions for heat transfer in nanoscale materials with dimensions shorter than the mean free path of phonons l_{MFP} [39, 40]. Therefore, the results obtained here imply that the strong phononic scattering at the interface may perturb the ballistic heat transport mechanism.

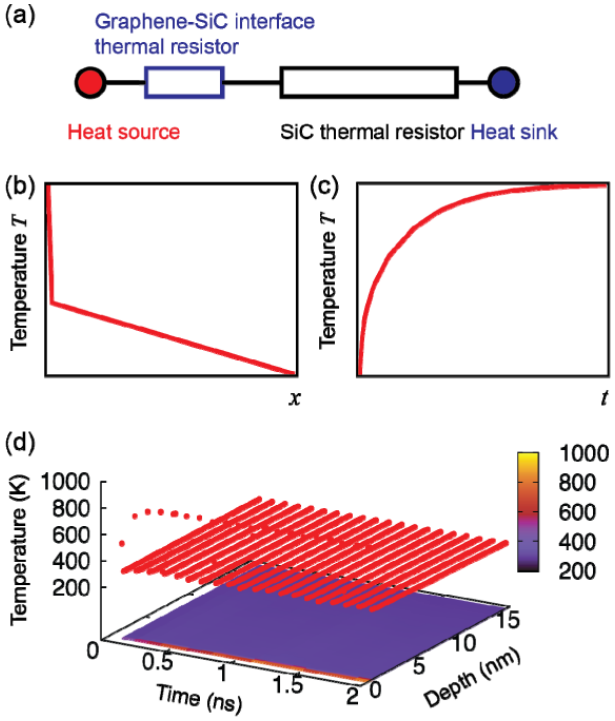

Figure 5. (a) Schematic illustration the two-resistor model. (b) and (c) The temperature profile $T(x)$ evolution $T_G(t)$ in the graphene sheet and 6H-SiC as predicted by using the Fourier's diffusive model for heat transfer. (d) The distribution and time evolution of temperature $T(x, t)$ in the hybrid graphene–SiC system at $P = 10$ GW m^{-2}, as a function of time t and depth x from the supported graphene into the substrate.

3.4. Interface engineering

Gas molecules such as O_2, NO, N_2 can be used to intercalate the graphene–substrate interface. They can successfully remove the rippling corrugation resulting from the lattice registry mismatch and symmetry breaking due to the strong electronic coupling [14]. Here we intercalate argon atoms into the interface with a density from 0 to 10 atoms nm^{-2}, up to fully monolayer coverage. Our non-equilibrium MD simulation results show that the intercalations only reduce the interfacial thermal conductivity by about 7.14%. The dependence of κ_c on the areal density of argon atoms are plotted in figure 6, which clearly shows that the intercalation layer reduces κ_c, and increasing the interface coverage improves κ_c. Experimentally, hydrogen termination on the SiC surface [15] or intercalating oxygen atoms [14] could also be realized. Moreover, a recent model study shows that bonding strength of the interface and pressure across can also modulate the interfacial heat transfer [41]. These modifications of the interface would thus be expected to electronically decouple the graphene sheet with substrate but does not reduce much the heat dissipation efficiency.

4. Conclusion

In summary, the transient process of heat dissipation from a graphene-based electronic device to the environment through interfacial coupling to the substrate is studied here through atomistic simulations. The results identify a two-step heat dissipation process including a heating process for hundreds of picoseconds and a steady state afterwards with a temperature difference across the interface. The heat dissipation efficiency significantly depends on the power density generated and interfacial thermal conductivity. Our results predicts a safety window of thermal load and duration that one graphene-based device could survive without breakdown, if only weakly interfaced to the substrate, e.g. through van der Waals interaction. Interface engineering by intercalating argon atoms is also explored, which shows that in contrast to covalently bonded interfaces, this interface could insulate the suspended graphene to the substrate electronically, but the capability to dissipate heat is not reduced as much. Principles for optimal design are provided with respect to the interface between nanostructures and the substrate, which is of key importance in design functional nanoelectronics, nanoelectromechanical devices and other applications including photovoltaic devices, where high performance and stability at high loads can be achieved simultaneously.

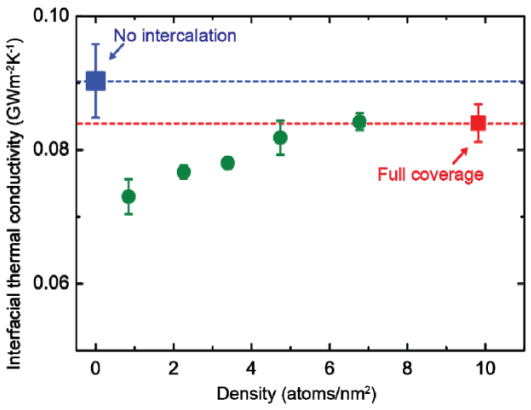

Figure 6. Interfacial thermal conductivity κ_c calculated for graphene layers intercalated with argon atoms, as a function of its areal density. κ_c without intercalation. The results for the case of full monolayer coverage are also plotted for reference.

Improved insights of the thermal dissipation process in graphene-based devices could be obtained by implementing a realistic model to simulate Joule heating in classical molecular dynamics. In contrast to the velocity-scaling approach used in this study, specifically phonon modes such as in-plane polarized ones undergo more direct heating from electron–phonon scattering. Also, spectral analysis of the graphene–substrate coupling could improve the understanding of observed phenomena [42, 43].

Acknowledgments

We acknowledge support from DARPA-NTI, and helpful discussions with Y Zhao and CL Chen (Teledyne Scientific) are appreciated. This research was also supported by the Tsinghua University Initiative Scientific Research Program 2011Z02174, the National Natural Science Foundation of

China through Grant 11002079, and the Tsinghua National Laboratory for Information Science and Technology, China. We also thank the anonymous reviewers whose suggestions helped significantly to improve the manuscript.

References

[1] Novoselov K S *et al* 2004 *Science* **306** 666
[2] Morozov S V *et al* 2006 *Phys. Rev. Lett.* **97** 016801
[3] Schedin F *et al* 2007 *Nature Mater.* **6** 652
[4] Kim K *et al* 2010 *Phys. Status Solidi (RRL)* **4** 302
[5] Freitag M *et al* 2009 *Nano Lett.* **9** 1883
[6] Chen Y C, Zwolak M and Di Ventra M 2003 *Nano Lett.* **3** 1691
[7] Jia X *et al* 2009 *Science* **323** 1701
[8] Girit C O *et al* 2009 *Science* **323** 1705
[9] Chen C *et al* 2009 *Nature Nanotechnol.* **4** 861
[10] Chae D-H *et al* 2009 *Nano Lett.* **10** 466
[11] Mak K F, Lui C H and Heinz T F 2010 *Appl. Phys. Lett.* **97** 221904
[12] Xu Z and Buehler M J 2009 *ACS Nano* **3** 2767
[13] Nagashima A, Tejima N and Oshima C 1994 *Phys. Rev.* B **50** 17487
[14] Sutter P, Sadowski J T and Sutter E A 2010 *J. Am. Chem. Soc.* **132** 8175
[15] Riedl C *et al* 2009 *Phys. Rev. Lett.* **103** 246804
[16] Xu Z and Buehler M J 2010 *J. Phys.: Condens. Matter* **22** 485301
[17] Chang S-W, Nair A K and Buehler M J 2012 *J. Phys.: Condens. Matter* **24** 245301
[18] Waldmann D *et al* 2011 *Nature Mater.* **10** 357
[19] Emtsev K V *et al* 2009 *Nature Mater.* **8** 203
[20] Tersoff J 1989 *Phys. Rev.* B **39** 5566
[21] Abraham F F and Batra I P 1989 *Surf. Sci.* **209** L125
[22] Berber S *et al* 2000 *Phys. Rev. Lett.* **84** 4613
[23] Kawamura T *et al* 2008 *Japan. J. Appl. Phys.* **47** 8898
[24] Lindsay L and Broido D A 2010 *Phys. Rev.* B **81** 205441
[25] Persson B N J, Volokitin A I and Ueba H 2011 *J. Phys.: Condens. Matter* **23** 045009
[26] Prasher R 2010 *Science* **328** 185
[27] Plimpton S 1995 *J. Comput. Phys.* **117** 1
[28] Liao A *et al* 2010 *Phys. Rev.* B **82** 205406
[29] Engelund M *et al* 2010 *Phys. Rev. Lett.* **104** 036807
[30] Müller-Plathe F 1997 *J. Chem. Phys.* **106** 6082
[31] Hu L, Desai T and Keblinski P 2011 *Phys. Rev.* B **83** 195423
[32] Nilsson O *et al* 1997 *High Temp. - High Pressures* **29** 73
[33] Yue Y, Zhang J and Wang X 2011 *Small* **7** 3324
[34] Chen Z *et al* 2009 *Appl. Phys. Lett.* **95** 161910
[35] Pop E *et al* 2007 *J. Appl. Phys.* **101** 093710
[36] Shinde S K and Goela J S 2006 *High Thermal Conductivity Materials* (Berlin: Springer)
[37] Mahan G D and Bartkowiak M 1999 *Appl. Phys. Lett.* **74** 953
[38] Wilson R B and Cahill D G 2012 *Phys. Rev. Lett.* **108** 255901
[39] Chen G and Yang R 2002 *ASME Conf. Proc.* **2002** 61
[40] Shiomi J and Maruyama S 2006 *Phys. Rev.* B **73** 205420
[41] Shen M *et al* 2011 *Phys. Rev.* B **84** 195432
[42] Ong Z-Y and Pop E 2010 *J. Appl. Phys.* **108** 103502
[43] Chalopin Y *et al* 2012 *Phys. Rev.* B **85** 195302